

Article

Dynamics of Cylindrical Parts for Vibratory Conveying

Nicola Comand ¹ and Alberto Doria ^{2,*}

¹ Department of Management and Engineering, University of Padova, 36100 Vicenza, Italy; nicola.comand@phd.unipd.it

² Department of Industrial Engineering, University of Padova, 35131 Padova, Italy

* Correspondence: alberto.doria@unipd.it; Tel.: +39-049-827-6803

Received: 20 January 2020; Accepted: 06 March 2020; Published: 11 March 2020

Featured Application: Motion of cylindrical parts in conveyors.

Abstract: Vibratory conveyors are widely used to feed raw materials and small parts to processing equipment. Up to now, most of the research has focused on materials and parts that can be modeled as point masses or small blocks. This paper focuses on the conveying of cylindrical parts. In this case, the rolling motion is an essential feature of conveyor dynamics. First, the dynamic equations governing the rolling motion are stated, and the effects of friction and rolling resistance coefficients on the behavior of the system are analyzed. Then, a non-linear numerical model is developed in MATLAB. It takes into account the transition between pure rolling and rolling with sliding and the impacts of the cylindrical part on the edges of the conveyor. Numerical results showing the effect of the operative parameters of the conveyor and of friction properties on the traveled distance are presented and discussed. Finally, a comparison between numerical and experimental results is presented.

Keywords: vibration; conveyor; friction; rolling; non-linear simulation

1. Introduction

The automation of industrial processes very often requires the handling of small [1–3] and micro items [4], which include mechanical and electrical components used in the assembly processes, finite products that have to be packaged, and raw materials that have to be processed. In many industrial scenarios, these small items have to be transported, oriented, and sorted. Nowadays, vibratory systems are very common, because they allow handling small items in a versatile and efficient way. They have a simple and sturdy construction and are suited to handle dusty and hot materials as well. For these reasons, some researchers have studied the kinematics and dynamics of vibratory conveying, orienting, and sorting. In 1963, Taniguchi et al. [5] carried out a pioneering study that highlighted the role of friction and clearly stated the differences between the gliding and hopping motions of a machine part on a vibrating conveyor, in which the machine part was considered a point mass. The influence of directional friction characteristics was analyzed in [6], assuming a point mass model of the vibrating part. In [7], the mechanical part was modeled as a rigid body with six degrees-of-freedom (DOFs) and the contact mechanics were deeply analyzed; however, the rolling motion was neglected, since a block-shaped component was studied. The dynamics of a block moving along the spiral track of a vibratory bowl feeder were studied in [8], and the block was modeled as a point mass. Some recent studies dealt with the design of the conveyor [9–11]; also in these studies, the part was modeled as a point mass, and no rolling motion was considered.

Cylindrical parts, similar to pins and plugs, are very common in electrical and mechanical industry; also, a screw is better represented by a cylinder than by a block. Other manufacturing processes require the handling of cylindrical and quasi-cylindrical parts, e.g., the pharmaceutical industry has to convey cylindrical pills and phials. Cylindrical parts are processed by classical conveyors, if their axes of rotation form a small angle with the direction of conveying [12]. When this condition is not satisfied, they begin to roll down the track. Most of the scientific literature dealing with conveyors neglects this rolling motion [1], because sometimes, this phenomenon does not have a significant effect on the process. For example, in orientation processes, often a cylindrical part that can roll also has a wrong orientation and it has to be rejected both if it slides and if it rolls. Nevertheless, in some applications, the cylindrical part has to travel a larger distance, and the rolling motion strongly influences the process.

Thus, this paper focuses on the dynamics of cylindrical parts in a vibrating conveyor, with the aim of explaining the basic differences between the vibration conveying of a block and of a rolling cylinder. The scientific literature in this field is rather scarce. Some papers [13,14] analyzed the probabilities of natural resting aspects of cylinders and parts with curved surfaces in vibratory bowl feeders. In [15], a preliminary numerical analysis of the motion of a cylindrical part on a conveyor was carried out, and the possibility of rolling, sliding, and hopping motions was highlighted. This paper is an extension of the previous research [15] that includes analytical studies, a more detailed mathematical model that considers impacts, and a wide parametric analysis.

The paper is organized as follows. First, the dynamic equations governing the rolling motion of a cylindrical part are analytically derived, the differences between vibratory conveying of rolling and non-rolling parts are highlighted, and the parameters with the largest influence on the rolling motion are found. Then, a two-dimensional (2D) non-linear numerical model is developed that takes into account the transition between pure rolling and rolling with sliding and the impacts of the cylindrical parts with the edge of the conveyor. Series of numerical simulations are carried out, which show the effects of variations in the system's parameters on the motion of the cylindrical part. Finally, testing equipment composed of a vibrating conveyor and a vision system that monitors the motion of a cylinder is presented. Numerical results are compared with experimental results, and the benefits and limits of 2D simulations are discussed.

2. Theoretical Basis

There are very important differences between the vibration conveying of parts that can roll on the conveyor track and parts that cannot roll. A 2D model with the plane of motion perpendicular to the axis of the cylinder is enough to point out these differences.

Vibration conveying of non-rolling parts is a dynamic phenomenon dominated by dry friction. Figure 1a shows a small block on the track of the conveyor, which is tilted by angle θ with respect to the horizontal direction. A fixed reference frame with axis x parallel to the track and axis y perpendicular to track is introduced. R_x and R_y are the components of the reaction force exerted by the track surface on the block (the positive direction is represented); they are related by the static Coulomb friction coefficient μ_s and by the kinetic Coulomb friction coefficient μ_c . Acceleration (\vec{a}) of the conveyor is tilted by angle ψ with respect to the conveyor track. If the motion of the conveyor is harmonic with amplitude x_0 and angular frequency ω , the components of the acceleration are:

$$A_x = a \cos(\psi) = -x_0 \omega^2 \sin(\omega t) \cos(\psi) \quad (1)$$

$$A_y = a \sin(\psi) = -x_0 \omega^2 \sin(\omega t) \sin(\psi). \quad (2)$$

Angle ψ is essential for the vibration conveying of non-rolling parts. When acceleration has the direction shown in Figure 1a, the inertia force adds to the weight of the block, the reaction force R_y is large, the modulus of the demanded tangential reaction force $|R_x|$ is smaller than the maximum static friction force ($\mu_s |R_y|$), and the block cannot slide backwards. Conversely, when acceleration \vec{a} changes its direction, the inertia force tends to cancel the weight force, R_y decreases, and the modulus of the demanded tangential reaction force $|R_x|$ may become larger than the maximum

static friction force; hence, the block moves, and forwards sliding begins. This condition repeats at every period of the harmonic motion and eventually the block moves forwards with respect to the track.

The scenario drastically changes when the part has a cylindrical shape, as depicted in Figure 1b. A stop-plate is introduced, and R_n is the reaction force exerted by the stop plate on the cylinder (the positive direction is represented), M_r is the rolling resistance torque (the positive direction is represented), m is the cylinder mass, and mg is the gravity force (the actual direction is represented).

First, the cylindrical part is assumed to be steady on the vibrating conveyor, and the dynamic conditions that make possible the beginning of the relative motion are analyzed. The equations of motion in the x and y directions are:

$$ma_x = -mgsin(\theta) + R_x + R_n \tag{3}$$

$$ma_y = -mgcos(\theta) + R_y. \tag{4}$$

In Equations (3) and (4), a_x and a_y are the two components of the acceleration of the center of mass of the cylindrical part.

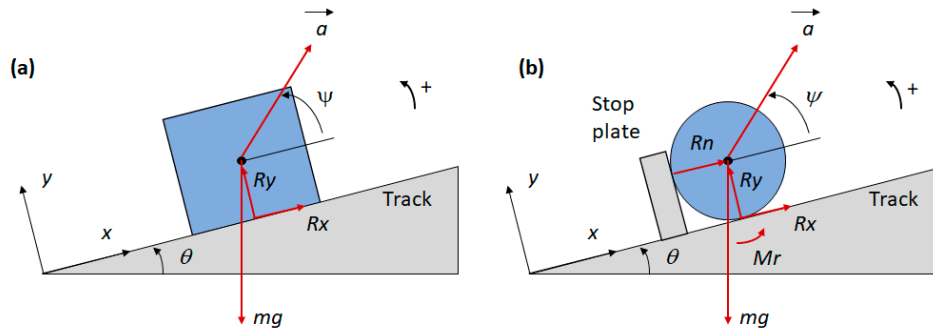


Figure 1. Block (a) and cylindrical part; (b) on the vibrating conveyor.

When there is no relative motion, a_x and a_y coincide with the components of acceleration of the conveyor (A_x and A_y); therefore, the equations of motion become:

$$macos(\psi) = -mgsin(\theta) + R_x + R_n \tag{5}$$

$$ma sin(\psi) = -mgcos(\theta) + R_y. \tag{6}$$

The perpendicular reaction force can be calculated from Equation (6).

$$R_y = ma sin(\psi) + mgcos(\theta) \tag{7}$$

The contact between the cylinder and the track is unilateral; hence, $R_y \geq 0$. When R_y tends to zero, the cylinder separates from the track, and the hopping motion begins. The hopping motion can be avoided decreasing the vibration acceleration, and this solution leads to a noise reduction [9]. Thus, this kind of motion is not considered in the framework of this research.

The angular momentum equation about the center of mass of the cylindrical part is:

$$I_G \ddot{\phi} = r R_x - u_{rs} R_y sgn(\dot{\phi}). \tag{8}$$

Reaction force R_n does not appear in Equation (8), because it passes through the center of mass of the cylinder. I_G is the moment of inertia about the center of mass, r is the cylinder radius, u_{rs} is the coefficient of rolling resistance in static condition, $\ddot{\phi}$ is the angular acceleration, $\dot{\phi}$ is the angular velocity, and sgn is the signum function. Since the beginning of the rolling motion is considered, $\dot{\phi} = 0$ and $sgn(\dot{\phi}) = -1$, because after the beginning of relative motion, a negative rolling velocity will take place: $\dot{\phi} = -v_r/R$. Tangential reaction force R_x can be calculated from the angular momentum equation:

$$R_x = -\frac{u_{rs}}{R} R_y. \tag{9}$$

The term $\frac{u_{rs}}{R}$ is the non-dimensional rolling friction coefficient in static condition, which is named f_{vs} .

The reaction force that the stop plate exerts on the cylinder (R_n) can be calculated from Equations (5) and (9). The contact between the cylinder and the stop plate is unilateral ($R_n > 0$). Hence, the condition $R_n \leq 0$ in conjunction with the adoption of the maximum rolling friction coefficient in Equation (9) defines the beginning of the relative motion between the cylinder and the conveyor track:

$$R_n = m a \cos(\psi) + m g \sin(\theta) + f_{vs} R_y \leq 0, \tag{10}$$

If Equation (6) is introduced into Equation (10), the following condition for the beginning of rolling motion is obtained:

$$\frac{a}{g} \leq -\frac{\sin(\theta) + f_{vs} \cos(\theta)}{\cos(\psi) + f_{vs} \sin(\psi)}. \tag{11}$$

Figure 2 depicts the values of the static rolling friction coefficient (f_{vs}) that prevents the rolling motion against non-dimensional acceleration (a/g) for parametric values of ψ . Only negative values of acceleration are considered, since a negative acceleration is required to begin the rolling motion; the maximum value of non-dimensional acceleration is $a/g = -\sin(\theta)/\cos(\psi)$, since for larger values, the resultant of the gravity and inertia forces pushes the cylinder against the stop plate.

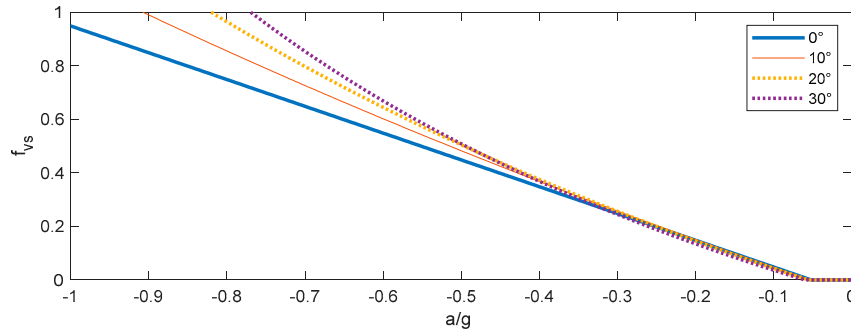


Figure 2. Static rolling friction coefficient that prevents the rolling motion, $\theta = 3^\circ$ and parametric values of ψ .

Figure 2 shows that very large and unrealistic values [16] of static rolling friction coefficient (f_{vs}) are needed to prevent the beginning of the rolling motion. When a/g is lower than -0.35 , the increase in angle ψ increases the value of f_{vs} .

Hypothetically, the cylindrical part excited by conveyor vibrations could begin a sliding motion as well. The following condition for the beginning of the sliding motion can be derived:

$$\frac{a}{g} \leq -\frac{\sin(\theta) + \mu_s \cos(\theta)}{\cos(\psi) + \mu_s \sin(\psi)}. \tag{12}$$

It is worth noticing that this condition is the same that holds true for non-cylindrical parts [1]. Equation (12) is similar to Equation (11), but f_{vs} is substituted by μ_s , which is the static Coulomb friction coefficient. For most of the materials used in industrial applications [16], the static Coulomb friction coefficient is much larger than the non-dimensional rolling friction coefficient in static condition. Therefore, the negative acceleration needed to begin the sliding motion is much larger (in modulus) than the one needed to begin the rolling motion.

The evolution of the rolling motion is now analyzed. The equations of motion are:

$$m a_x = -m g \sin(\theta) + R_x \tag{13}$$

$$m A_y = -m g \cos(\theta) + R_y \tag{14}$$

$$I_G \ddot{\varphi} = r R_x - f_v R R_y \operatorname{sgn}(\dot{\varphi}). \tag{15}$$

Moreover, during pure rolling, the following kinematic condition has to be fulfilled:

$$\ddot{\varphi} = -\frac{a_x - a \cos(\psi)}{R}. \tag{16}$$

R_y can be calculated from Equation (14); then, Equations (13), (15), and (16) can be solved to calculate R_x , a_x , and $\ddot{\varphi}$. Taking into account that for a cylinder $I_G = 0.5mR^2$, the following results are obtained:

$$R_x = \frac{1}{3} m(a \cos(\psi) + g \sin(\theta)) + \frac{2}{3} f_v R_y \operatorname{sgn}(\dot{\varphi}) \tag{17}$$

$$a_x = \frac{1}{3} a \cos(\psi) - \frac{2}{3} g \sin(\theta) + \frac{2}{3} f_v \frac{R_y}{m} \operatorname{sgn}(\dot{\varphi}) \tag{18}$$

$$\ddot{\varphi} = -\frac{1}{R} \left(\frac{2}{3} (-a \cos(\psi) - g \sin(\theta) + f_v \frac{R_y}{m} \operatorname{sgn}(\dot{\varphi})) \right). \tag{19}$$

It is worth noticing that when the cylinder rolls forwards ($\dot{\varphi} < 0$), the rolling friction term in Equation (19) adds to the gravity term. The motion of the cylinder on the conveyor track can be studied integrating Equations (18) and (19); the input is $a \cos(\psi)$. Generally speaking, a numerical integration is needed (see Section 3) owing to the sgn function. Nevertheless, $f_v < 0.01$ in most industrial processes, and an approximation of the integrals of Equations (18) and (19) can be obtained assuming $f_v = 0$.

According to Equation (11), the forward motion begins when $a/g \leq -\sin(\theta)/\cos(\psi)$. Since in normal conveying applications angle θ is rather small, another simplification can be made assuming that the forward rolling motion begins when $a \cos(\psi) = -x_0 \omega^2 \sin(\omega t) \cos(\psi)$ becomes negative. This assumption simplifies the initial conditions, because in the harmonic motion vibration, the acceleration changes its sign when the displacement is zero and the velocity has the maximum positive value ($x_0 \omega$).

The integration of Equation (18) with the above-mentioned simplifications and initial conditions leads to the following equations for the absolute velocity (v_x) and displacement (x) of the center of mass of the cylinder:

$$v_x = \frac{1}{3} \omega x_0 \cos(\omega t) \cos(\psi) + \frac{2}{3} \omega x_0 \cos(\psi) - \frac{2}{3} g \sin(\theta) t \tag{20}$$

$$x = \frac{1}{3} x_0 \sin(\omega t) \cos(\psi) + \frac{2}{3} \omega x_0 \cos(\psi) t - \frac{1}{3} g \sin(\theta) t^2. \tag{21}$$

From the point of view of conveying, the most important parameter is the relative velocity v_r between the part and the track of the conveyor:

$$v_r = v_x - \omega x_0 \cos(\omega t) \cos(\psi) \tag{22}$$

$$v_r = \frac{2}{3} \omega x_0 \cos(\psi) - \frac{2}{3} \omega x_0 \cos(\omega t) \cos(\psi) - \frac{2}{3} g \sin(\theta) t. \tag{23}$$

The relative velocity includes a positive and constant term due to initial velocity ($x_0 \omega$); a harmonic term due to the vibration of the conveyor plate, whose integral over a period ($T = 2\pi/\omega$) is zero; and a negative term due to gravity that increases (in modulus) with time.

If $\theta = 0$ (horizontal conveying), the average conveying velocity in the period (\bar{v}_r) is constant and equal to $\frac{2}{3} \omega x_0 \cos(\psi)$. If $\theta > 0$ the average conveying velocity decreases, and at the n th period it assumes the value:

$$\bar{v}_r = \frac{2}{3} \left(\omega x_0 \cos(\psi) - g \sin(\theta) \frac{\pi}{\omega} (2n - 1) \right) \quad n = 1, 2, \dots, N. \tag{24}$$

When \bar{v}_r becomes negative, the cylindrical part rolls backwards and eventually impacts the stop plate. Figure 3 depicts the ratio between \bar{v}_r and the maximum vibration speed ($x_0 \omega$) versus period number (n) for $\theta = 3^\circ$. In Figure 3a, the ratio between the vibration acceleration and gravity acceleration (a/g) is 1 and the parametric values of angle ψ are considered; the increase in ψ has a

negative effect on the conveying speed. In Figure 3b, ψ is set to zero, and the parametric values of the ratio a/g are considered; the increase in vibration acceleration has a positive effect on vibration conveying.

Equation (24) holds true with the assumption $f_v = 0$. If rolling resistance is present, it contributes to decreasing the average conveying speed in the period.

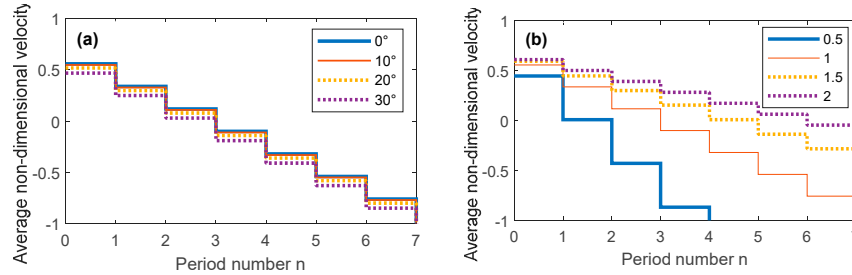


Figure 3. Average non-dimensional conveying velocity ($\bar{v}_r/x_0\omega$) versus period number, $\theta = 3^\circ$, $a/g = 1$ and parametric values of ψ (a); $\psi = 0$ and parametric values of a/g (b).

During pure rolling motion, the reaction force R_x given by Equation (17) is needed to guarantee equilibrium. $|R_x|$ has to be smaller than the maximum static friction force ($\mu_s R_y$). Hence, the ratio $|R_x|/R_y$ has the meaning of static friction coefficient needed to guarantee equilibrium during pure rolling. Figure 4 shows the ratio $|R_x|/R_y$ against non-dimensional acceleration (a/g) for $\theta = 3^\circ$, $f_v = 0$ and parametric values of ψ .

With $\psi = 0$, the friction coefficient needed to guarantee the pure rolling motion is only slightly influenced by the versus of acceleration.

With $\psi > 0$, the friction coefficient needed to guarantee the pure rolling motion is significantly smaller when the conveyor acceleration is positive than when acceleration is negative. This phenomenon happens because when acceleration changes sign, the decrease in reaction force R_y (Equation (7)) is not compensated by the decrease in R_x (Equation (17)), and this effect becomes even more important when ψ is large. Since in most industrial material μ_s is in the range of $0.6 \div 1$ [1], the transition from a pure rolling motion to a rolling with sliding can take place only in the presence of large negative accelerations of the vibration conveyor.

When the cylindrical part rolls backwards, it may impact the stop plate; in this case, the equation of motion in the x direction becomes:

$$ma_x = -mgsin(\theta) + R_x + F_{imp} \tag{25}$$

in which F_{imp} is the impact force, which has the same direction of R_n in Figure 1. F_{imp} strongly increases R_x ; hence, the ratio $|R_x|/R_y$ may reach very large values, and the sliding motion can begin.

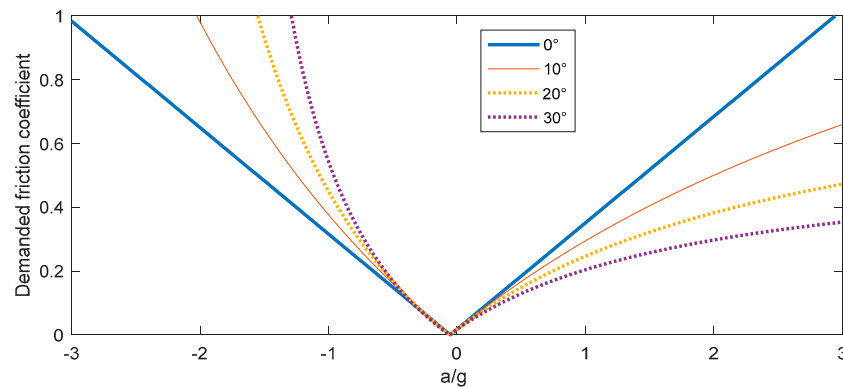


Figure 4. Friction coefficient needed to guarantee the pure rolling motion, $\theta = 3^\circ$, $f_v = 0$, and parametric values of ψ .

3. Numerical Model

The simulation of the motion of a cylindrical part on a vibrating plane is not a simple task due to the non-linear phenomena that take place, e.g., the frequent transition between states of motion and the impacts with the stop plate. In order to address the problem, a combination of a MATLAB (R2019b, MathWorks Inc., Natick MA, USA, 2020) script and its simulation environment Simulink was adopted. The simulations are started from a main MATLAB script which initializes the variables at the initial conditions: the cylinder is touching the track and in contact with the stop plate, as depicted in Figure 1b. The cylinder is supposed to start with a pure rolling motion; therefore, the main script launches a Simulink simulation, which implements this case. When a proper dynamic condition is met, the simulation is stopped and the simulation of rolling with sliding motion is started by the main script. Such simulation is stopped when particular kinematic and dynamic conditions are met. The process is iterated until the desired simulation duration is reached.

The block diagram of the simulation is represented in Figure 5. The two transition conditions require special attention, because they rule the simulation. The transition from pure rolling to rolling with sliding is ruled by a dynamic condition. When the tangential reaction force R_x needed to guarantee the equilibrium of the pure rolling motion (Equation (17)) is larger than the maximum static friction force, the MATLAB main script stops the Simulink rolling model and starts the Simulink sliding model.

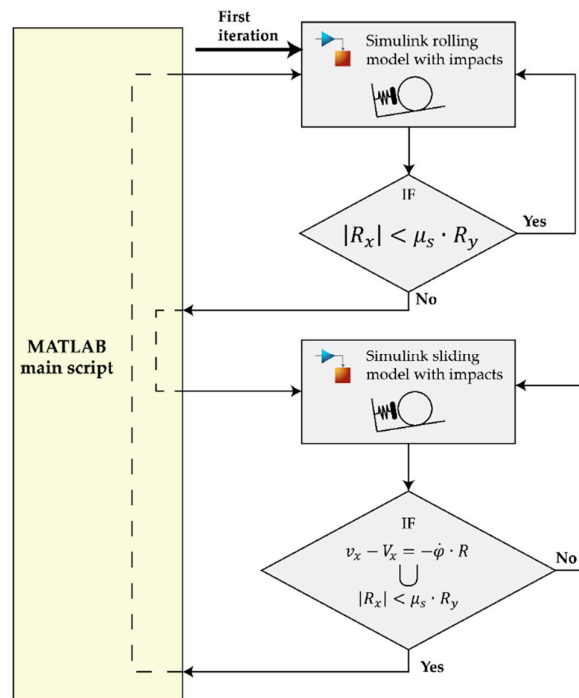


Figure 5. Logical flow of the simulation.

The MATLAB main script stops the Simulink sliding model when a dynamic and a kinematic condition are satisfied at the same time. The kinematic condition is the pure rolling condition, which is given by Equation (26).

$$v_x - V_x = -\dot{\phi} \cdot R \tag{26}$$

This equation shows when there is a possible switching from rolling with sliding to pure rolling, but a dynamic condition is to be satisfied as well. This condition states that the tangential reaction force has to be smaller than the maximum static friction force.

One of the novelties of this numerical model with respect to previous papers [15] is the introduction of the impacts with the stop plate, which makes the integration of the equations more

complex. Impact forces are calculated representing contact stiffness by means of a lumped spring, which is compressed only if the distance between the cylinder and the stop plate is smaller than a fixed threshold. For this reason, the simulation environment Simulink was chosen, which proved to be very intuitive for the integration of single sets of equations. Then, the problem was moved to the transition between the two cases. The development of a model entirely programmed in Simulink showed problems of flickering between different states and was not very effective. Therefore, it was decided to exploit the versatility of a simulation managed by a MATLAB script at the highest level with the power of the Simulink simulation environment at a lower level. The results lived up to expectations, although troubleshooting and a fine tuning of the parameters of the Simulink solver was needed.

4. Numerical Results

Numerical simulations aimed at exploring the dynamics of vibration conveying of cylindrical parts beyond the limits of the analytical model of Section 2. In particular, numerical simulations made it possible to analyze the effect of the impacts of the cylindrical part on the stop plate.

A realistic reference case was defined, which is characterized by the following parameters of the vibratory conveyor: $x_0 = 0.0002$ m, $\omega = 314$ rad/s (frequency 50 Hz), $\theta = 3^\circ$, $\psi = 0^\circ$. The maximum modulus of conveyor acceleration is 19.72 m/s² ($a/g = 2$).

The rolling part has a radius $r = 0.007$ m and mass $m = 0.096$ kg. The friction parameters are $f_v = 0.005$, $\mu_c = 0.3$, and $\mu_s = 0.6$. The value of the rolling resistance is more than twice that of the typical rolling elements of bearings [16] and takes into account that the cylindrical part may be rough or dirty. The kinetic Coulomb friction coefficient value is inside the typical range of values found in vibratory conveyors [1,6,9]. The static Coulomb friction coefficient was set to be twice the kinetic coefficient [17]. Finally, the impact stiffness was set to $k = 1,000,000$ N/m; this value made it possible to obtain values of contact forces similar to the measured ones (about $60 \div 80$ N).

The first parametric simulations aimed at analyzing the effect of angle ψ ; Figure 6 shows numerical results in terms of the absolute displacement of the cylinder center of the mass. In the same figure, for comparison, the displacement of the conveyor is represented (along the direction tilted by ψ with respect to the x axis).

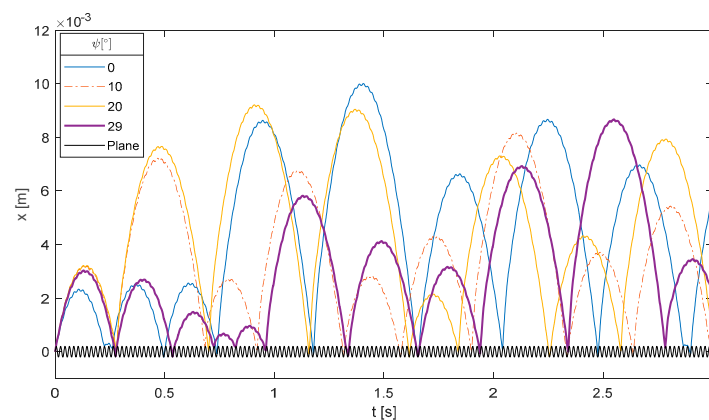


Figure 6. Numerical results, displacement of the cylindrical part along the track, $\theta = 3^\circ$, $f_v = 0.005$, $\mu_c = 0.3$, $\mu_s = 0.6$, and parametric values of ψ .

In the plots of Figure 6, two different phases can be identified. The first phase (phase 1), which ends at about 0.25 s and includes 10 \div 12 vibration periods, is the initial motion of the cylindrical part without impacts. As foreseen by theoretical analysis, the cylindrical part begins its motion at $t = 0$ owing to the initial velocity given by the conveyor, reaches the maximum displacement, and eventually impacts the stop plate. The maximum displacement is rather small (about 0.003 m), and this value is in agreement with the theoretical predictions (Equation (21)).

In this phase, the increase in the angle ψ up to 20° leads to an increase in the traveled distance, a further increase leads to a reduction in the traveled distance. This particular behavior is due by the presence of two opposite effects.

The first effect can be understood looking at the sliding velocity (v_{sl}) of the cylindrical part:

$$v_{sl} = v_x - V_x + R\dot{\phi} \tag{27}$$

which is plotted in Figure 7 with conveyor acceleration. If $\psi = 0$, the cylindrical part slides both when the conveyor acceleration is negative and positive (forwards and backwards sliding, respectively). Backwards sliding causes a reduction in the traveled distance. This phenomenon is in agreement with the analytical results of Figure 4, which show that for $\psi = 0$, the static friction coefficient needed to guarantee the pure rolling motion is larger than $\mu_s = 0.6$ both for negative (-2) and for positive (+2) values of non-dimensional acceleration.

Conversely, Figure 7 shows that if ψ increases, there is only forwards sliding, since the static friction coefficient is able to prevent backwards sliding when the conveyor acceleration becomes positive, and the cylindrical part behaves similar to a block. It is worth noticing that this behavior is in agreement with the analytical results of Figure 4.

The second effect is the decrease in the initial velocity of the cylindrical part when ψ increases; see Equation (20). In summary, for small values of ψ , the first effect is dominant, and the traveled distance increases, whereas for large values of ψ , the second effect reduces the traveled distance.

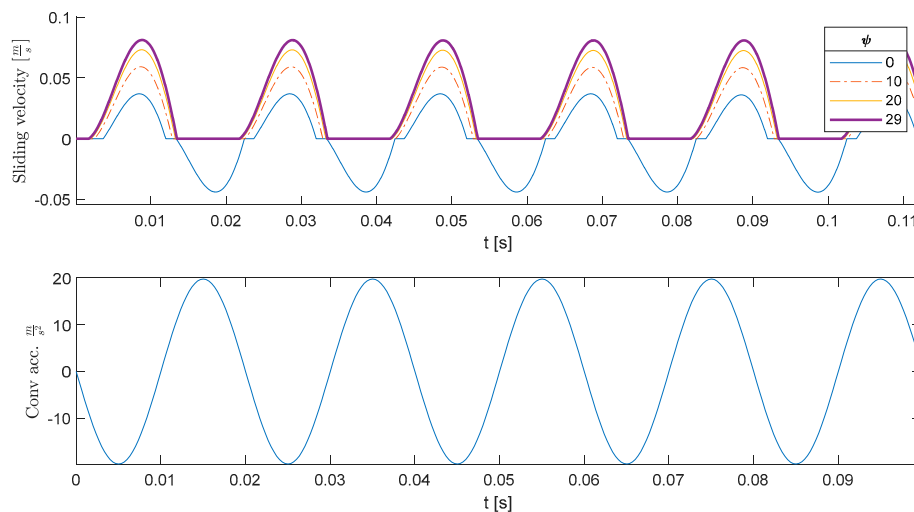


Figure 7. Numerical results, sliding velocity of the cylindrical part along the track, $t < 0.1$ s, $\theta = 3^\circ$, $f_v = 0.005$, $\mu_c = 0.3$, $\mu_s = 0.6$, and parametric values of ψ .

The second phase of the motion (phase 2, $t > 0.25$ s) is dominated by the impacts of the cylindrical part on the stop plate.

The cylindrical part reaches the maximum displacement in this phase, and this value chiefly depends on impact mechanics. If the relative velocity (Equation (22)) is large, because the cylindrical part and the conveyor move in opposition, the conveyor transfers a lot of energy to the cylindrical part, which has a large rebound after the impact. This phenomenon occurs at $t = 2.04$ for $\psi = 0^\circ$. Figure 8, which is a zoom of Figure 6 of about $t = 2.04$ s, shows that the impact occurs when the conveyor has the maximum positive velocity, whereas the velocity of the cylindrical part is negative. Conversely, if the relative velocity is small, because the cylindrical part and the conveyor move in phase, the conveyor transfers less energy to the cylindrical part, and a smaller rebound occurs. This phenomenon takes place at $t = 0.49$ s for $\psi = 0^\circ$, since Figure 9 shows that the cylindrical part impacts the conveyor when it has a negative velocity.

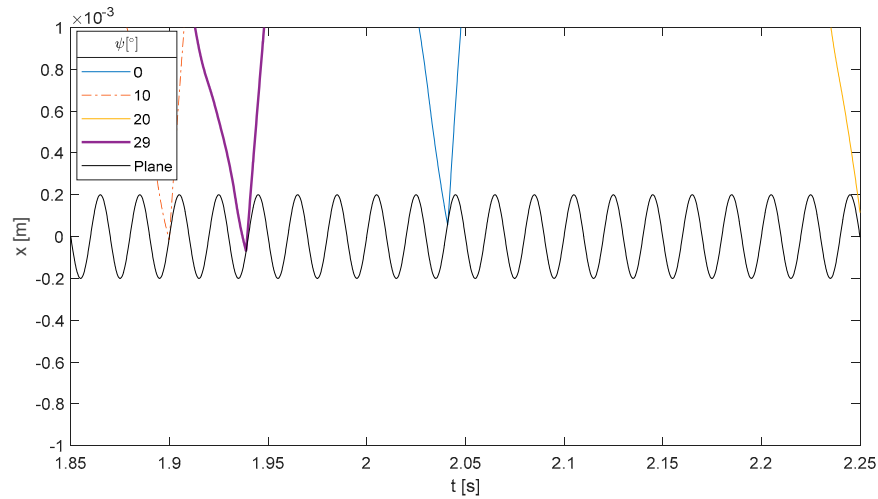


Figure 8. Numerical results, displacement of the cylindrical part along the track, impact with large relative velocity at $t = 2.04$, $\psi = 0^\circ$, $\theta = 3^\circ$, $f_v = 0.005$, $\mu_c = 0.3$, $\mu_s = 0.6$.

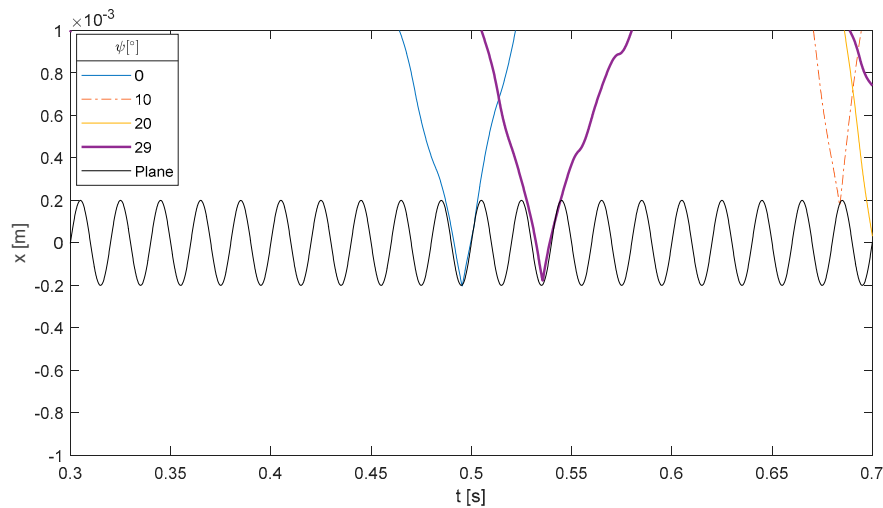


Figure 9. Numerical results, displacement of the cylindrical part along the track, impact with small relative velocity at $t = 0.49$, $\psi = 0^\circ$, $\theta = 3^\circ$, $f_v = 0.005$, $\mu_c = 0.3$, $\mu_s = 0.6$.

The angle of conveyor acceleration (ψ) has a negligible effect on the second phase (impact dominated) of the motion of the cylindrical part on the conveyor, since the relative velocity at the impact depends much more on the previous motion than on conveyor maximum velocity, which slightly decreases if ψ increases. Actually, after some impacts, the relative velocity at the impact changes randomly. Thus, the motion of the cylindrical part on the conveyor is similar to the motion of a bouncing ball that impacts a vibrating table, which may exhibit a chaotic behavior [18,19].

Figure 10 shows for the same cases of Figure 6 the sliding velocity of the cylindrical part and highlights that, owing to the large value of non-dimensional acceleration ($a/g = 2$), very often the cylinder slides on the conveyor track. The largest sliding velocities take place just after the impacts.

The second parametric simulation aimed at analyzing the effect of conveyor vibration frequency. Conveyor acceleration was kept equal to the previous value ($a/g = 2$); therefore, an increase in frequency led to a decrease in velocity according to this equation:

$$v = \frac{a}{\omega}. \tag{28}$$

Figure 11 clearly shows that the increase in the frequency has a negative effect on the motion of the cylindrical part both before and after the first impact. The first effect takes place because the initial

velocity is smaller, while the second effect takes place because the relative velocity at the impact is smaller. If the vibration frequency decreases to 25 Hz, the traveled distance increases up to 0.043 m. It is worth noticing that even if the dynamics of conveying of block-shaped parts and cylindrical parts are very different, the decrease in vibration frequency has a positive effect in both cases [1].

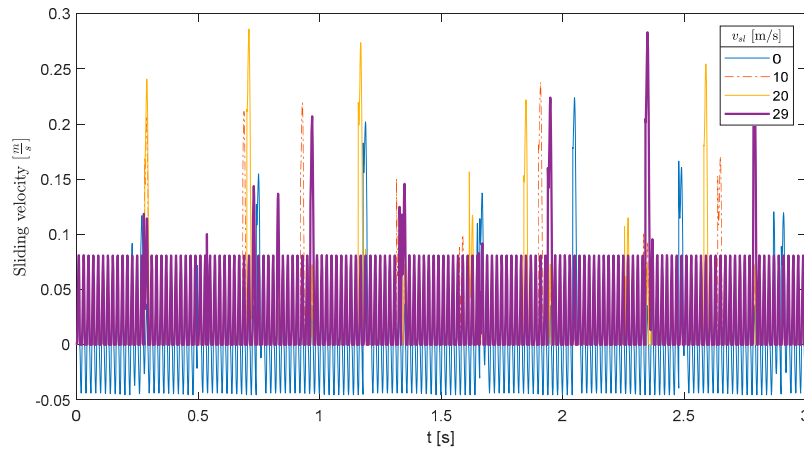


Figure 10. Numerical results, sliding velocity of the cylindrical part along the track, $\theta = 3^\circ$, $f_v = 0.005$, $\mu_c = 0.3$, $\mu_s = 0.6$, and parametric values of ψ .

Then, the effect of rolling friction coefficient was investigated by means of numerical simulations. The results, which are presented in Figure 12, show that realistic variations in f_v have a negligible effect on the conveying of cylindrical parts. Before the first impact (phase 1), the decrease in f_v causes a very small increase in the traveled distance. After the first impact (phase 2), the variation in the rolling friction coefficient changes the instants in which the most energetic impacts take place, but the traveled distance does not significantly change.

Figure 13 shows the effect of contact stiffness on the conveying of cylindrical parts. The contact stiffness does not affect phase 1, and it does not have a clear effect on the traveled distance in phase 2. This phenomenon agrees with physical intuition, because the contact stiffness is another factor that contributes to randomly varying the relative velocity at the impact, which is the main factor influencing the rebound of the cylindrical part.

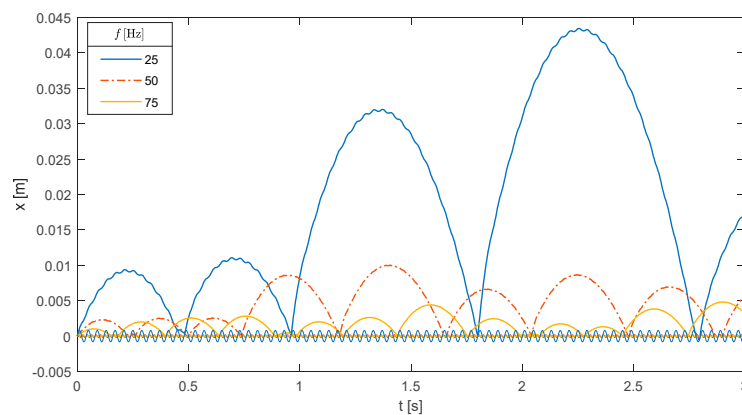


Figure 11. Numerical results, displacement of the cylindrical part along the track, $\theta = 3^\circ$, $\psi = 0^\circ$, $f_v = 0.005$, $\mu_c = 0.3$, $\mu_s = 0.6$, and parametric values of frequency.

Finally, the effect of friction coefficients was investigated.

Figure 14 shows that μ_s has a small effect on phase 1: if the static friction coefficient increases above 0.6, the traveled distance increases. This phenomenon can be explained looking at Figure 15, which shows the sliding speed for the same values of μ_s . With $\mu_s = 1$ during phase 1, the cylinder

does not slide at all, and the traveled distance increases, since the pure rolling motion dissipates less energy than the rolling with sliding motion. It is worth noticing that this result agrees with the analytical results of Figure 4.

After the first rebound, the impacts take place at random instants and, again, the relative velocity at the impact has the largest effect.

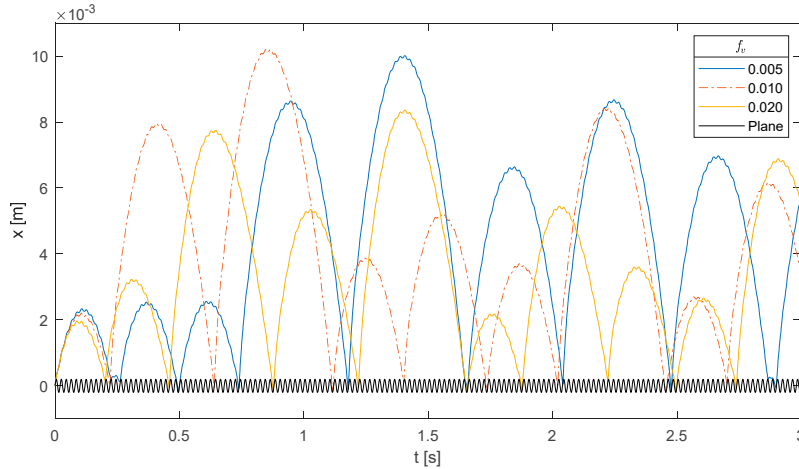


Figure 12. Numerical results, displacement of the cylindrical part along the track, $\theta = 3^\circ$, $\psi = 0$, $\mu_c = 0.3$, $\mu_s = 0.6$, and parametric values of f_v .

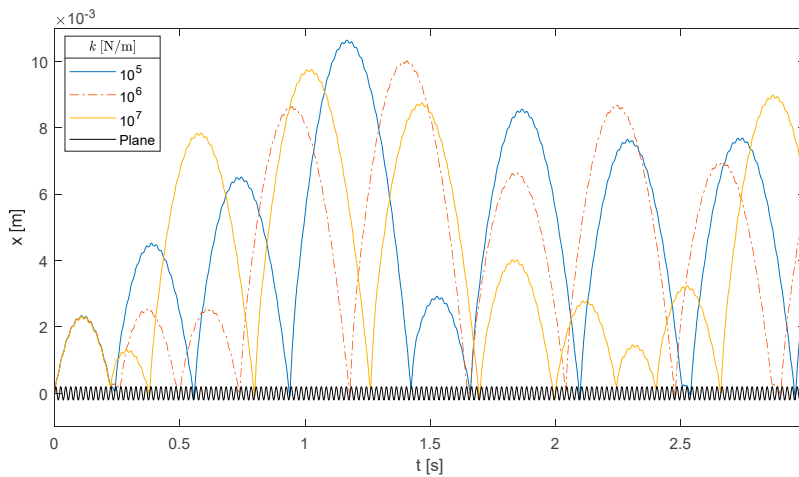


Figure 13. Numerical results, displacement of the cylindrical part along the track, $\theta = 3^\circ$, $\psi = 0$, $f_v = 0.005$, $\mu_c = 0.3$, $\mu_s = 0.6$, and parametric values of contact stiffness.

The effect of a proportional variation of both friction coefficients (μ_c and μ_s) is presented in Figure 16. In phase 1, the cylinder with the highest μ_s reaches the largest distance because it rolls without sliding, as shown in Figure 17. After the first impact (phase 2), the motion is dominated by the relative velocity at the impact; nevertheless, a decrease in μ_c leads to an average increase in the traveled distance. With $\mu_c = 0.2$, there are 4 rebounds with a traveled distance larger than 0.008 m, whereas with $\mu_c = 0.4$, there is no rebound with a traveled distance larger than 0.008 m. This phenomenon occurs because for every value of μ_c and μ_s , there are large sliding velocities (Figure 17) after the impacts, and a reduction in μ_c leads to a reduction in energy dissipation.

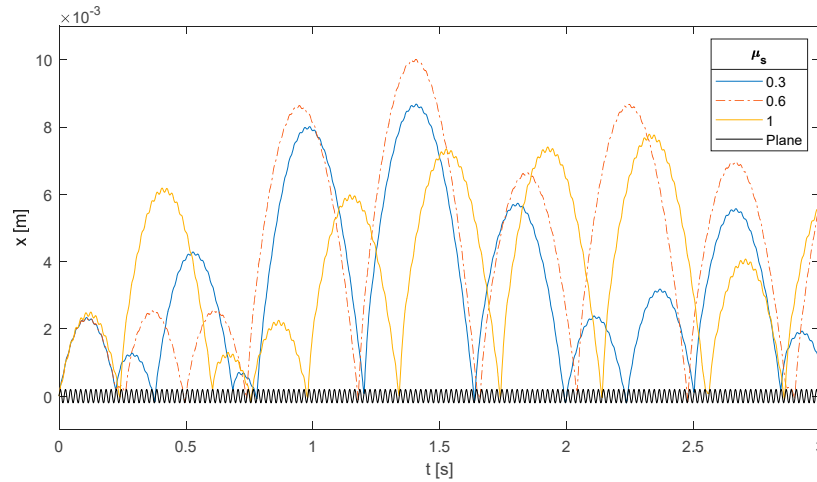


Figure 14. Numerical results, displacement of the cylindrical part along the track, $\theta = 3^\circ$, $\psi = 0$, $f_v = 0.005$, $\mu_c = 0.3$, and parametric values of static friction coefficient μ_s .

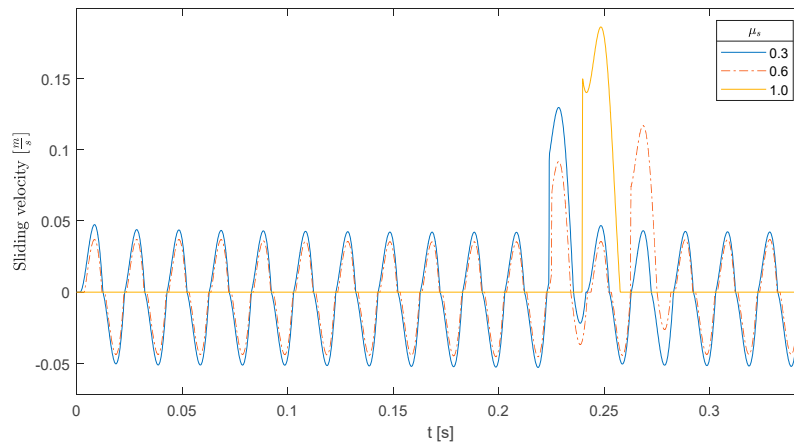


Figure 15. Numerical results, sliding velocity of the cylindrical part along the track, $\theta = 3^\circ$, $\psi = 0$, $f_v = 0.005$, $\mu_c = 0.3$, and parametric values of static friction coefficient μ_s .

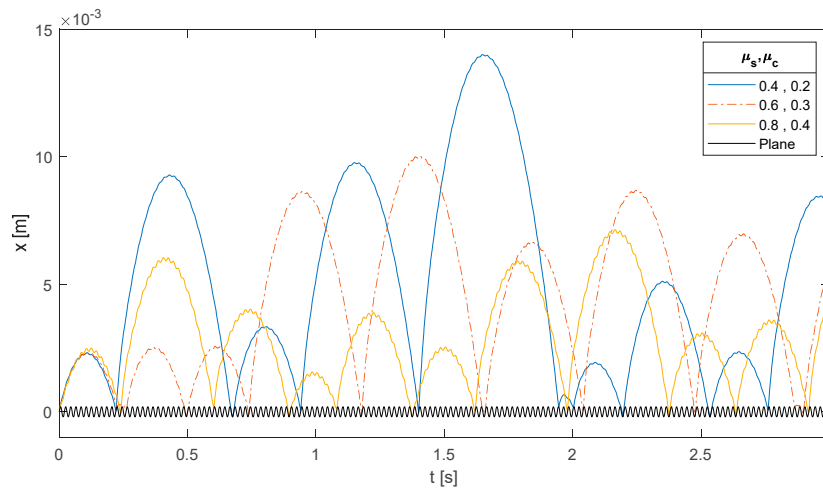


Figure 16. Numerical results, displacement of the cylindrical part along the track, $\theta = 3^\circ$, $\psi = 0$, $f_v = 0.005$, and parametric values of static friction coefficients μ_c and μ_s .

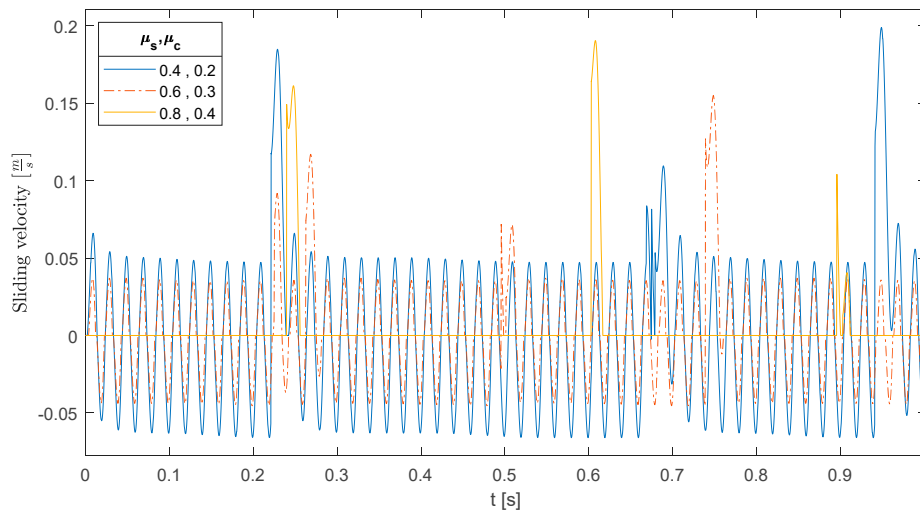


Figure 17. Numerical results, sliding velocity of the cylindrical part along the track, $\theta = 3^\circ$, $\psi = 0$, $f_v = 0.005$, and parametric values of static friction coefficients μ_c and μ_s .

The numerical results presented in this section clearly highlight that only the decrease in the vibration frequency can significantly increase the distance traveled by the cylindrical part. Nevertheless, even the largest traveled distances foreseen by simulations (0.043 m), which corresponds to about six times the cylinder radius, is not enough to cover the distances requested in many automatic manufacturing processes. For this reason, the development of a saw-teeth grooved surface of the conveyor track is highly recommended (see Figure 18). In this case, a traveled distance equal to $5 \div 6$ times the cylinder radius is enough to move the cylindrical part from one groove to the following groove and to generate a sequential motion.

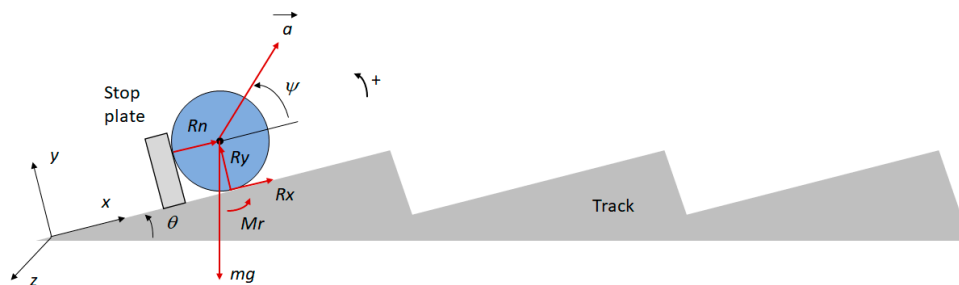


Figure 18. Conveyor with saw-teeth track.

5. Comparison between Numerical and Experimental Results

In order to validate the numerical model, some experimental tests were carried out at the Laboratory of Robotics and Mechatronics of Padova University, which is equipped with the linear vibratory conveyor shown in Figure 19.

A track (120 mm long) with a stop plate was printed with additive manufacturing and mounted on the conveyor. A single steel cylinder was placed on the track. The motion was monitored by an AVT Pike f-032b camera with a frame-rate of 470 frames/s. Both the track and the cylinder were equipped with markers that were used to reconstruct their trajectories, using the Hough transform [20]. The static friction coefficient of the cylinder on the track was measured as well, and resulted in $\mu_s = 0.7$.

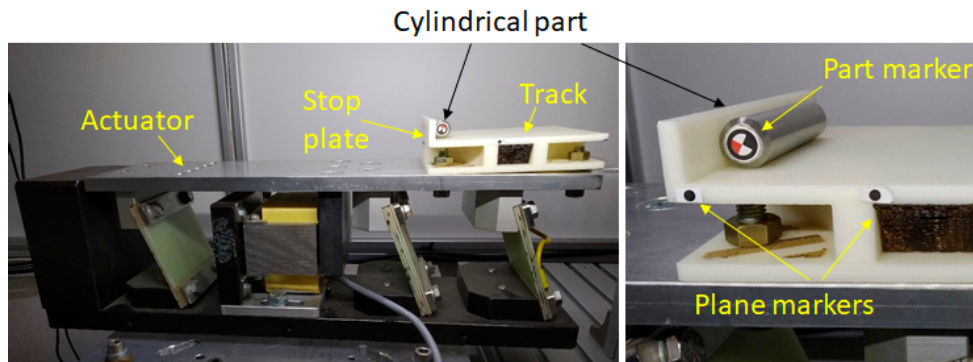


Figure 19. Vibratory conveyor for experimental tests.

Figure 20 makes a comparison between numerical and experimental results. The numerical model is able to capture the most important features of cylinder motion, since the experimental results show a sequence of chaotic rebounds of the cylinder on the stop plate. The largest rebounds predicted by the numerical model have about the same duration (0.5 s) of experimental rebounds, and the traveled distances are only a bit larger ($\approx 10\%$) than the measured values. This phenomenon may occur because, owing to the three-dimensional geometry of the system, the cylinder velocity may have a small component in the transverse direction (z in Figure 18).

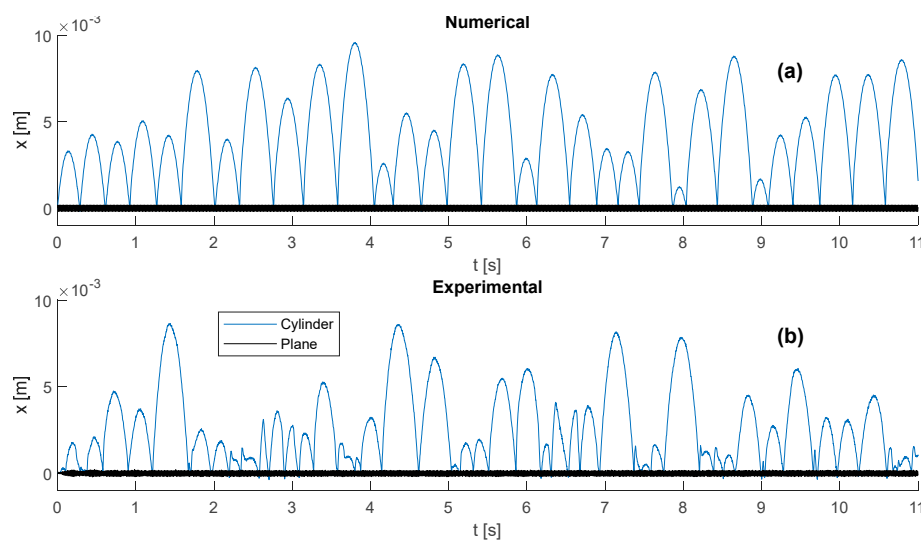


Figure 20. Comparison between numerical (a) and experimental (b) results. $\theta = 3^\circ$, $\psi = 10^\circ$, $f = 55$ Hz, $a/g = 2.254$, $k = 1000000$ N/m, $f_v = 0.005$, $\mu_c = 0.35$ and $\mu_s = 0.7$.

The main difference between numerical and experimental results is that the numerical model predicts a smaller number of bad impacts, with a short rebound. This happens because the numerical model is two-dimensional and assumes an impact between the cylinder and the stop plate along a line. In reality, the system is three-dimensional, and often the contact begins when a corner of the cylinder impacts the stop plate. The energy transfer from the conveyor to the cylinder is less efficient and leads to a reduced traveled distance.

These phenomena could be analyzed by means of a 3D numerical model, which would be much more complex and cumbersome than the presented 2D model (a 2D simulation lasting 1 s requires a computation time of about 16 s). Nevertheless, it is worth noticing that a complete agreement between numerical and experimental results could be difficult to achieve even with a 3D simulation, since the system is non-linear and chaotic; thus, small differences between simulation and experimental parameters may lead to large differences in results [19,21]. In actual conveyors, there are many cylindrical parts, and their collisions further enhance the chaotic behavior of the system [22].

6. Conclusions

The dynamics of vibratory conveying of cylindrical parts are very different from the dynamics of conveying of block-shaped parts. Both analytical and numerical calculations showed that large distances cannot be traveled owing to the backwards rotation of the cylindrical part.

The impacts of the cylindrical part on the stop plate are an essential feature of this kind of motion and strongly increase the traveled distance. After some rebounds, the impacts of the cylindrical part on the stop plate of the vibratory conveyor take place at random instants, which correspond to random values of the relative velocity between the cylindrical part and the stop plate. The impacts with the largest relative velocity lead to the largest rebounds. Eventually, the motion becomes chaotic.

Numerical simulations made it possible to investigate the effect of the most important parameters on the vibratory conveying of cylindrical parts. When vibration acceleration is kept constant, a decrease in vibration frequency leads to a relevant increase in the traveled distance. The kinetic friction coefficient (μ_c) influences the traveled distance; when μ_c halves, the maximum traveled distance almost doubles. The other parameters have a small or negligible effect on the conveying process. This phenomenon occurs because the energy transferred by the impacts to the cylindrical part essentially depends on the relative velocity between the part and the stop plate, and the variations in ψ , f_v , k and μ_s have a small effect on the relative velocity but influence the instants in which the strongest impacts (with large relative velocity) take place.

Author Contributions: Conceptualization, N.C. and A.D.; methodology, N.C. and A.D.; software, N.C.; validation, N.C. and A.D.; formal analysis, N.C. and A.D.; investigation, N.C. and A.D.; writing—Original draft preparation, N.C. and A.D.; writing—Review and editing, N.C. and A.D.; supervision, A.D. All authors have read and agreed to the published version of the manuscript.

Funding: This research received no external funding.

Conflicts of Interest: The authors declare no conflict of interest.

References

- Boothroyd, G. *Assembly Automation and Product Design*, 2nd ed.; Taylor & Francis: Boca Raton, FL, USA, 2005; pp. 29–45.
- Rosati, G.; Faccio, M.; Barbazza, L.; Rossi, A. Hybrid flexible assembly systems (H-FAS): Bridging the gap between traditional and fully flexible assembly systems. *Int. J. Adv. Manuf. Technol.* **2015**, *81*, 1289–1301.
- Rosati, G.; Faccio, M.; Finetto, C.; Carli, A. Modelling and optimization of Fully Flexible Assembly Systems (F-FAS). *Assem. Autom.* **2013**, *33*, 165–174.
- Kritikou, G.; Aspargathos, N. Micro—manipulation methods and assembly of hexagonal microparts on a programmable platform with electrostatic forces. *Int. J. Mech. Control* **2019**, *20*, 71–80.
- Taniguchi, O.; Sakata, M.; Suzuki, Y.; Osanai, Y. Studies on vibratory feeder. *Bull. ISME* **1963**, *6*, 37–43.
- Okabe, S.; Yokoyama, Y.; Boothroyd, G. Analysis of vibratory feeding where the track has directional friction characteristics. *Int. J. Adv. Manuf. Technol.* **1988**, *3*, 73–85.
- Wolfsteiner, P.; Pfeiffer, F. Modeling, simulation, and verification of the transportation process in vibratory feeders. *ZAMM-J. Appl. Math. Mechanics/Zeitschrift für Angewandte Mathematik und Mechanik*, **2000**, *80*, 35–48.
- Vilán, J.V.; Robleda, A.S.; Nieto, P.J.G.; Placer, C.C. Approximation to the dynamics of transported parts in a vibratory bowl feeder. *Mech. Mach. Theory* **2009**, *44*, 2217–2235.
- Ma, H.W.; Fang, G. Kinematics analysis and experimental investigation of an inclined feeder with horizontal vibration. *Proc. Inst. Mech. Eng. Part C J. Mech. Eng. Sci.* **2016**, *230*, 3147–3157.
- Buzzoni, M.; Battarra, M.; Mucchi, E.; Dalpiaz, G. Motion analysis of a linear vibratory feeder: Dynamic modeling and experimental verification. *Mech. Mach. Theory* **2017**, *114*, 98–110.
- Despotović, Z.; Šinik, V.; Janković, S.; Dobrilović, D.; Bjelica, M. Some specific of vibratory conveyor drives. In Proceedings of the V International Conference Industrial Engineering and Environmental Protection 2015 (IIZS 2015), Zrenjanin, Serbia, 15–16 October 2015.
- Edmondson, N.F.; Redford, A.H. Flexible parts feeding for flexible assembly. *Int. J. Prod. Res.* **2001**, *33*, 2279–2294.

13. Boothroyd, G.; Ho, C. Natural resting aspects of parts for automatic handling. *Trans. ASME J. Eng. Ind.* **1977**, *1977*, 314–317.
14. Lee, S.G.; Ngoi, B.K.A.; Lye, S.W.; Lim, L.E.N. An Analysis of the Resting Probabilities of an Object with Curved Surfaces. *Int. J. Adv. Manuf. Technol.* **1996**, *12*, 366–369.
15. Comand, N.; Boschetti, G.; Rosati, G. Vibratory feeding of cylindrical parts: A dynamic model. In *Advances in Italian Mechanism Science*; Carbone, G., Gasparetto, A., Eds.; Springer: Berlin/Heidelberg, Germany, 2019; pp. 203–210.
16. Juvinall, R.C.; Marshek, K.M. *Fundamentals of Machine Component Design*; Wiley & Sons: Hoboken, NJ, USA, 2006; pp. 559–563.
17. Williams, G. *Engineering Tribology*; Cambridge University Press: Cambridge, UK, 2005; pp. 145–147.
18. May, R.M. Simple mathematical models with very complicated dynamics. *Nature* **1976**, *261*, 459–467.
19. Tufillaro, N.B.; Albano, A.M. Chaotic dynamics of a bouncing ball. *Am. J. Phys.* **1986**, *54*, 939–944.
20. Russ, J.C. *The Image Processing Handbook*; CRC Press: Boca Raton, FL, USA, 2016.
21. Naylor, M.A.; Sanchez, P.; Swift, M.R. Chaotic dynamics of an air-damped bouncing ball. *Phys. Rev. E* **2002**, *66*, 057201.
22. Lee, C.-W.; Seireg, A.; Duffy, J. Chaotic behavior of a two mass bouncing system. In Proceedings of 18th Annual ASME Design Automation Conference, Scottsdale, AZ, USA, 13–16 September 1992.



© 2020 by the authors. Licensee MDPI, Basel, Switzerland. This article is an open access article distributed under the terms and conditions of the Creative Commons Attribution (CC BY) license (<http://creativecommons.org/licenses/by/4.0/>).